Postprint of: Ducka A., Trawiński B., Bochentyn B., Dubiel A., Kusz B., Structure and thermoelectric properties of nickel-doped copper selenide synthesised in a hydrogen atmosphere, Materials Research Bulletin, Vol. 133 (2021), 111042, DOI: 10.1016/j.materresbull.2020.111042

STRUCTURE AND THERMOELECTRIC PROPERTIES OF NICKEL-DOPED COPPER SELENIDE SYNTHESISED IN A HYDROGEN ATMOSPHERE

A. Ducka[1], B. Trawiński[1,*], B. Bochentyn[1], A. Dubiel[2], B. Kusz[1]

[1] *Gdańsk University of Technology, Faculty of Applied Physics and Mathematics, ul. Narutowicza 11/12, 80-233 Gdańsk*

[2] *AGH University of Science and Technology, Faculty of Materials Science and Ceramics, al. Mickiewicza 30, 30-059 Kraków*

Corresponding author: Bartosz Trawiński
Gdańsk University of Technology, Faculty of Applied Physics and Mathematics, Solid State Physics Department, ul. G. Narutowicza 11/12, 80-233 Gdańsk, Poland
E-mail address: bartosz.trawinski@pg.edu.pl

ABSTRACT

Nickel-doped copper selenide—$Cu_{2-x}Ni_xSe$ (x=0; 0.01; 0.02; 0.03)—materials with high thermoelectric properties were synthesised through reduction of reagents in hydrogen. The impact of the nickel content on both the microstructure and thermoelectric properties was examined. The nickel-doped samples' microstructure differed significantly from pristine copper selenide. Besides Cu_2Se, copper precipitations were present in the materials. The presence of the metallic nanoparticles in the nickel-doped materials enhanced the electrical conductivity without significantly changing the Seebeck coefficient. Above 500 K, the structure of the doped samples also resulted in decreased thermal conductivity. Also, the impact of the Cu_2Se phase transition on thermoelectric properties is visible. The highest ZT value, equal to 0.8 at 650 K, was reached for the $Cu_{1.98}Ni_{0.02}Se$ sample.

KEYWORDS:

Thermoelectric materials; copper selenide; reduction of reagents; thermoelectric figure of merit

GRAPHICAL ABSTRACT

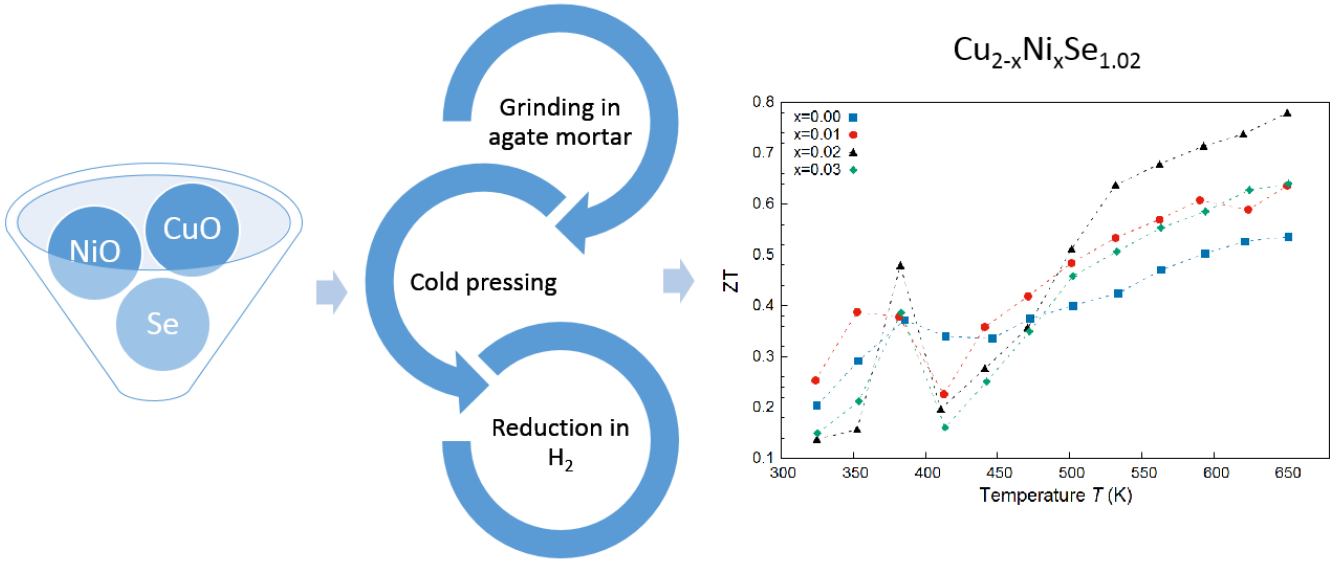

HIGHLIGHTS:

- $Cu_{2-x}Ni_xSe$ (x=0; 0.01; 0.02; 0.03) synthesis by reduction in hydrogen
- Nickel doping has little influence on the Seebeck coefficient
- Enhancement of σ is observed
- Metallic precipitations resulting from Ni doping enhanced ZT

1. INTRODUCTION

Thermoelectric materials are gaining more and more attention due to their potential application in devices directly converting waste heat into electricity [1].

Thermoelectric devices are characterised by many advantages, e.g. they are environmentally friendly, have small size, and can be used simultaneously with other devices to improve their efficiency by recovering the waste heat [2]. However, the application of thermoelectric devices is not very common because of the high cost and long production process. Also, the efficiency of the thermoelectric materials themselves remains a challenge. Fortunately, this field is continuously progressing, which is resulting in enhancements of the thermoelectric properties as well as cost reductions of the technology.

The quality of a thermoelectric material is characterised by the dimensionless figure of merit, ZT, given by Eq. (1):

$$ZT = \frac{S^2\sigma}{\kappa}T, \tag{1}$$

where S is the absolute Seebeck coefficient, σ is the electrical conductivity of the sample, κ is the total thermal conductivity, and T is the absolute temperature. The total thermal conductivity consists of lattice component κ_{lat} and electrical component κ_{el}, which depends directly on the electrical conductivity by the Wiedemann-Franz law. Ideally, to obtain the best thermoelectric performance, it is necessary to maximally enhance both the Seebeck coefficient and the electrical conductivity, resulting in the power factor ($S^2\sigma$) being as high as possible. At the same time, the total thermal conductivity should be as low as possible. Unfortunately, all of these parameters are linked, which makes enhancing the properties of the material a challenge. A compromise between all of the parameters needs to be reached to enhance the ZT. What is more, it is important to underline that it is more beneficial that the materials show a high average ZT across a wide temperature range than to have a high value of maximum ZT in a narrow span [1].

Many materials have been examined because of their potentially excellent thermoelectric performance. Among them, some of the most known are: Bi-Te alloys [3,4], Half-Heusler compounds [5,6], PbTe [7,8], SnSe [9,10], and skutterudites [11]. Copper chalcogenides, especially copper selenide, are also attracting more and more interest among researchers due to their low thermal conductivity, which results in high ZT values [12–15]. Cu_2Se appears in the form of two different phases: the low-temperature phase known as α-Cu_2Se, and β-Cu_2Se, which exists at high temperatures (>400K). Despite its apparently simple chemical formula, copper selenide has a complex crystal structure. There is no total agreement on the space group of α-Cu_2Se [13,16]. At approximately 400 K, a reversible phase transition to β-Cu_2Se occurs. The high-temperature phase crystallises in a Fm-3m space group, with the selenium atoms forming a FCC sublattice, and highly mobile copper ions, which behave like an ionic liquid [16]. During the transition, the crystalline grains remain unchanged, only the Cu ions are unfixed from their positions [17]. The high mobility of the copper ions results in a decrease of the phonon mean path which lowers the thermal conductivity [15]. The properties of high-temperature copper selenide are in agreement with the phonon liquid, electron crystal (PLEC) concept [14]. However such superionic behaviour has its disadvantages as well, for example, the high rate of Cu^+ migration which may decrease the durability of the material under working conditions [18]. Another challenge that has to be met is selenium evaporation from the system [19]. Unfortunately, the highest ZT values are obtained at temperatures at which the selenium evaporation is significant and has to be taken into consideration.

Various dopants have been proposed to enhance the thermoelectric performance of copper selenide, for example, to improve its chemical stability [18], or increase the

Seebeck coefficient [20], or the electrical conductivity [21]. The foreign atoms are introduced to the system both on selenium and copper sites. It has been observed that the doping leads to significant enhancement of the ZT, even to over 2, which is one of the highest values of thermoelectric figure-of-merit. The highest ZT values were obtained by incorporating lithium (ZT of 1.5 at 1000K) [18], indium (ZT of 2.5 at 850K) [22], magnesium (ZT of 1.6 at 850K) [21], nickel (1.5 at 800 K) [23], and by mixing with graphene nanoplates (ZT~ 1.8 at 873 K) [24].

Various methods have been proposed to fabricate pure copper selenide as well as doped material, e.g. a conventional solid-state sintering method [25], high-temperature, high-pressure technology [26], melting followed by spark plasma sintering [23], and mechanical alloying [13,27]. In those methods, elemental copper and selenium of high-purity were used as raw materials for synthesis, which makes it more expensive and requires pure elements to be obtained. Many synthesis methods also use spark plasma sintering technology to densify the sample [23,24,27,28].

In this paper, the authors report the fabrication of nickel-doped copper selenide by the reduction of substrates in hydrogen. Nickel was chosen due to its similar atomic radius compared to copper and, as a dopant, it should easily incorporate into the Cu_2Se structure. Theoretically, nickel ions, having a higher valence state (+2) than copper (+1) in Cu_2Se should reduce the electrical conductivity of the material, in which the holes dominate as charge carriers. However, Peng et al. [23] reported the opposite relation in their work and noticed an enhancement in conductivity with increasing nickel-doping. At the same time, the thermal conductivity was reduced by nickel incorporation. Another work on doping copper selenide with nickel at a low temperature showed that samples with higher nickel content have a slightly lower ZT than undoped copper selenide below room temperature [29]. What is more, doping

with immobile ions may reduce the Cu-migration as has already been reported for iron ions in another copper chalcogenide [15].

The presented work aimed to obtain nickel-doped copper selenide by an easy and low-temperature method which doesn't need expensive materials as substrates. The method of reduction of reagents in hydrogen can be used for this purpose as this approach reduces the cost of synthesis. It has already been successfully used to obtain other thermoelectric materials [30–32]. Moreover, the investigation of nickel-doping and its impact both on the structure and thermoelectric properties are presented.

2. EXPERIMENTAL

The nickel-doped copper selenide—$Cu_{2-x}Ni_xSe$ (x=0; 0.01; 0.02; 0.03)—samples were fabricated by the reduction of reagents in hydrogen. A sample without nickel was produced as reference material. Reagents of high purity were used for synthesis: copper oxide (CuO, Reachim), nickel oxide (JMC 895), and elemental selenium (Alfa Aesar). A 2% excess of selenium was applied to minimise its deficit in the final product due to evaporation from the system during synthesis. The appropriate amounts of CuO, NiO, and Se were mixed, ground in an agate mortar for approximately 10 min and then cold-pressed into pellets (ø=12 mm) under a uniaxial pressure of ~350 MPa. Subsequently, the prepared samples were reduced in an atmosphere of flowing hydrogen at 400°C for 2h. After the reduction, the samples were ground, cold-pressed and reduced under the same conditions. The third step consisted of grinding and pressing as the previous ones. The sintering time was extended to 12 h and the temperature was reduced to 350°C. The grinding and pressing were performed three times to obtain a homogeneous structure and to

provide a good dispersion of the elements. A previous study of reduction in a Bi-Te system [33] showed that even a single-step process allowed for a complete reduction of oxides, and intermetallic phase formation. A red deposit, a result of the evaporation of selenium, was found on the inner surface of the quartz tube in which the reduction took place.

The phase composition of the fabricated samples was investigated by the XRD method (Bruker D2 Phaser) with CuKα radiation (λ=1.542 Å) at room temperature. The HighScore Plus 3.0.2 software by PANalytican was used to analyse the diffraction patterns, and the LeBail method [34] was applied.

The microstructure and morphology of the investigated materials were analysed by an FEI Quanta FEG 250 SEM (Scanning Electron Microscope) with a secondary electron detector operating in high vacuum mode with an accelerating voltage of 10 kV. A quantitative elemental composition analysis using an EDX detector (Energy Dispersive X-ray spectroscopy) by EDAX Genesis APEX 2i with an ApolloX SDD spectrometer was performed.

The electrical conductivity and Seebeck coefficient were measured simultaneously using the four-probe method with a Linseis LSR-3 equipment. The measurements were performed in a helium atmosphere over the temperature range of 30–380 °C with 5-°C steps. The uncertainty of measurement declared by the producer is ±5%.

Thermal diffusivity D was measured by Laser Flash Analysis (LFA 457 MicroFlash, Netzsch) with a HgCdTe detector under an argon flow of 20 cm^3/min over a temperature range of 50–380 °C with 30 °C steps. The uncertainty of the measurement is ±7%. Density ρ of the samples, as well as the porosity, was

determined with the Archimedes method. Total thermal conductivity κ_{tot} was calculated from Eq. (2):

$$\kappa_{tot} = D \cdot \rho \cdot c_p, \quad (2)$$

where c_p is the specific heat capacity value based on the Dulong-Petit law.

3. RESULTS AND DISCUSSION

3.1. Phase and structural composition

To determine the phase composition of the obtained materials, powder XRD measurements were performed. The XRD patterns are shown in Figure 1. The main phase present in samples is orthorhombic α-Cu_2Se (Powder Diffraction File 47-1448) which can be identified as a low-temperature phase. The high-temperature β-Cu_2Se phase with a cubic crystal structure was not identified. Some diffraction peaks which can be attributed to copper can be found as well. This is consistent with the results of the EDX elemental analysis presented in Table 2. A significant excess of copper, resulting from the evaporation of selenium during the synthesis, was found. Additionally, a TGA measurement was performed to investigate possible Se evaporation during measurements of the samples' properties. The powdered sample was heated up to 673 K at a heating rate of 1 K/min. Above 523 K, a 1.77% mass decrease was observed. During the second TGA thermal cycle, the mass decreased by 0.94%. All doped samples had a nickel content similar to their nominal composition.

The Le Bail method was used to analyse the unit cell parameters of the compounds. The calculated values are shown in table 1. The lattice parameters and the cell volume of the nickel-doped materials are smaller than those of the pristine Cu_2Se.

This observation agrees with the smaller atomic radius of Ni when compared to Cu. The ratio of the cell volume between the $Cu_{1.99}Ni_{0.01}Se$ and the undoped material, equal to 0.992, agrees with that published for the β phase in [23]. The $Cu_{1.97}Ni_{0.03}Se$ sample had a similar cell volume to the $Cu_{1.99}Ni_{0.01}Se$. This suggests, that in the case of the $Cu_{1.97}Ni_{0.03}Se$ sample, the actual amount of Ni in the structure was smaller than expected. In the case of the $Cu_{1.98}Ni_{0.02}Se$, this ratio was equal to 0.981. Considering Vegard's law, it can be concluded that the solubility limit was not exceeded. This limit is 2% at 703 K [35]. We can state that this value is similar at room temperature.

The selected SEM images of the Ni-doped Cu_2Se are shown in Fig. 2. It can be seen that all of the samples were porous. As is shown in Table 2, the porosities calculated from the Archimedes method were between 8% ($Cu_{1.99}Ni_{0.01}Se$) and 13% ($Cu_{1.98}Ni_{0.02}Se$). The structure of the reference sample differed significantly from the doped samples: it lacked flat flake-like crystallites. Only irregular agglomerates consisting of small grains were visible. The microstructures of the doped samples were marked by the presence of large flat flake-like structures which were at some places orientated parallel to each other, forming a layered structure. The difference in the granular structure originated from the presence of Ni particles. Nickel is a catalyst in synthesis procedures and enhances grains' growth [36].

Fig. 3 shows higher magnification SEM images of the samples. For x=0.01, agglomerating particles of approximately 20–50 nm in size are visible. For the sample with the highest nickel content, the particles were uniformly distributed in the structure covering the surface of the Cu_2Se crystallites. In the case of the x=0.02 sample, larger, 50–200 nm separate particles are visible. The results of the EDX point analysis indicate that these precipitations were rich in copper, compared to the

large grains, which were closer to the nominal composition. Traces of nickel were also found. The composition of the precipitations is in agreement with the XRD phase analysis, which showed the presence of metallic copper. The undoped samples were free from visible metallic particles, therefore their formation was a result of Ni doping.

3.2. Thermoelectric properties

Figure 4 shows the temperature dependence of the Seebeck coefficient on the temperature of the prepared $Cu_{2-x}Ni_xSe$ samples. The positive sign of S indicates the p-type conduction of the sample. A rapid decrease in the Seebeck coefficient value was observed at approximately 407 K, which was stated before to be the temperature of the transition from the α-phase to the β. Such a phenomenon is in agreement with other studies on copper selenide [14,15,26]. It is worth noticing that the values of Seebeck coefficient presented in this paper are higher than those obtained by other researchers [23,26,37]. The values differed significantly for the low-temperature phase, however in the high-temperature regime, only small differences were observed. Both the porosity and nickel doping had little influence on the Seebeck coefficient, which is in agreement with other studies [23,38]. The lowest values of Seebeck coefficient were reached at temperatures close to the phase transition. Above the phase transition temperature, the Seebeck coefficient of the undoped material was only a few per cent higher than those of the doped materials.

The temperature dependence of the electrical conductivity of the samples is shown in Fig. 5. The shape of the plot was similar for all measured samples: a rapid change of conductivity at the phase transition temperature (~410 K), the maximum value after this phase transition, and then a decrease with increasing temperature. However, some differences can also be observed. In the 350–400 K temperature range, the

doped samples had increased electrical conductivity. It is possible that the difference in the undoped sample's microstructure may also have had a strong influence on the observed phenomenon.

The decrease of electrical conductivity with temperature above 450 K in the Cu_2Se system complies with other studies [13,23,27,37]. However, the values differ between studies. The undoped Cu_2Se showed the lowest electrical conductivity in almost the whole analysed temperature range. Despite the sample's highest porosity, the highest values of electrical conductivity were observed for the $Cu_{1.98}Ni_{0.02}Se$ material, reaching a maximum value equal to 380 S/cm at 460 K. The highest electrical conductivity of this sample seems interesting because of its highest porosity. However, the porosity may have had less influence than the nickel content, which possibly determined the electrical properties. The electrical conductivity increased with increasing nickel content when it came to the x=0, x=0.01, and x=0.02 samples. Ni doping resulted in the increase of the charge carriers' concentration and, consequently, electrical conductivity. This effect was especially significant above a 1% addition [23]. Additionally, the presence of metallic particles increased the conductivity at the grains' surface. The distance between agglomerates (x=0.01) or particles (x=0.02) in these materials made hopping or tunnelling between particles neglectable. The similarity of the electrical properties of the x=0.01 and x=0.03 samples agrees with the abovementioned similar lattice parameters and Ni content in these materials.

3.3. Thermal conductivity

Fig. 6 shows the measured values of thermal conductivity versus temperature. In both the α-phase (<400 K) and the β-phase region, the values of thermal conductivity

decreased with temperature. At a temperature of approximately 400 K, a rapid increase was observed, which is in agreement with the previous studies presented in this paper, as the phase transition occurs at such a temperature. The biggest increase was observed for the x=0.02 and the x=0.03 as the thermal conductivity reached over 1 $W \cdot m^{-1} \cdot K^{-1}$. However, these samples also exhibited a more significant decrease of thermal conductivity with temperature, and at temperatures above 470 K, the $Cu_{1.98}Ni_{0.02}Se$ had the lowest thermal conductivity of approximately 0.45 $W \cdot m^{-1} \cdot K^{-1}$ at 650 K. The reference sample and the $Cu_{1.99}Ni_{0.01}Se$ (with the lowest Ni content) exhibited lower thermal conductivity below 470 K. The decreased values of thermal conductivity may have been a result of increased phonon scattering on the metallic particles. The presented values are lower than those obtained by other researchers studying nickel-doped copper selenide [23]. The low values of the thermal properties resulted from the liquid-like behaviour of the copper ions, as well as the nickel doping and porosity of the samples.

Fig. 7 shows the calculated values of the ZT, determined using the measured values of thermoelectric parameters. The highest ZT was observed for the $Cu_{1.98}Ni_{0.02}Se_{1.02}$ and reached 0.79 at approximately 650 K, which resulted from the highest power factor and the lowest thermal conductivity above 500 K. What is more, this sample also exhibited the fastest growth of the ZT in the β-phase regime, which was the result of significant reduction of thermal conductivity over a high-temperature range. The ZT of all samples had an upward tendency.

The presented values of ZT are lower than the values obtained in other studies on nickel-doped copper selenide [23]. However Peng et al. found a value of ZT about 0.8 at 650 K for the $Cu_{1.99}Ni_{0.01}Se$, while in this paper, a similar value was observed for the $Cu_{1.98}Ni_{0.02}Se$ sample. On the other hand, some differences can be found both

in the structure and resulting thermoelectric properties. The samples synthesised by reduction of reagents in hydrogen exhibited lower thermal conductivity, which may have resulted from the higher porosity of the samples [38]. Moreover, it seems possible to optimise the reduction conditions to get denser and more uniform samples and therefore to finally increase the obtained ZT values of these materials. Therefore, the described method of nickel-doped copper selenide synthesis should be considered promising and worthy of further attention.

4. CONCLUSIONS

Nickel-doped copper selenides were synthesised using the method of reagent reduction in a hydrogen atmosphere. The main phase present in all samples was a low-temperature orthorhombic α-Cu_2Se, however, diffraction peaks from copper were also observed. The latter is in agreement with the EDX analysis, which showed an excess of Cu in the investigated materials. The addition of nickel resulted in the formation of metallic nanoparticles on the grains' surfaces.

The measured densities of the samples were lower than the theoretical values, which may determine the electrical properties [38]. However, it was observed that the higher the porosity, the lower the thermal conductivity due to scattering of phonons on grain boundaries. The intermediate porosity may have had a positive influence on the overall thermoelectric properties.

Nickel doping enhanced the electrical conductivity of all of the samples when compared to the pristine copper selenide. The metallic precipitates in the Ni-doped materials resulted in increased electrical conductivity. At the same time, the thermal conductivity was decreased above 500 K, which was in the highest ZT range. Possibly, the metallic precipitates, especially on the flat grains, may have increased

the materials' ZT by increasing the surface electrical conductivity without increasing the phonon part of the thermal conductivity, due to their nanometre size. All of the samples had similar values of the Seebeck coefficient in the high-temperature phase. The optimal doping was found to be 2%. The highest value reached almost 0.8 at 650 K for the $Cu_{1.98}Ni_{0.02}Se$ sample. The impact of phase-transition was visible at about 410 K when the parameters significantly and rapidly changed.

To sum up, the reduction of reagents in hydrogen allowed copper selenide with a nickel dopant to be synthesised. The synthesis method is easy and requires low temperatures. The materials obtained by such synthesis have properties only slightly worse than those produced by other methods [23].

5. ACKNOWLEDGEMENTS

This work was supported by the National Science Centre Poland [grant number 2016/21/B/ST8/03193].

6. REFERENCES

[1] J. He, T.M. Tritt, Advances in thermoelectric materials research: Looking back and moving forward, Science (80-.). 357 (2017). doi:10.1126/science.aak9997.

[2] F.J. Disalvo, Thermoelectric cooling and power generation, Science (80-.). 285 (1999) 703–706. doi:10.1126/science.285.5428.703.

[3] B. Poudel, Q. Hao, Y. Ma, Y. Lan, A. Minnich, B. Yu, X. Yan, D. Wang, A. Muto, D. Vashaee, X. Chen, J. Liu, M. Dresselhaus, G. Chen, Z. Ren, High-Thermoelectric Performance of Nanostructured Bismuth Antimony Telluride Bulk Alloys, Science (80-.). 320 (2008). doi:10.1126/science.1155140.

[4] W. Xie, X. Tang, Y. Yan, Q. Zhang, T.M. Tritt, Unique nanostructures and enhanced thermoelectric performance of melt-spun BiSbTe alloys, Appl. Phys. Lett. 94 (2009) 1–4. doi:10.1063/1.3097026.

[5] G. Joshi, X. Yan, H. Wang, W. Liu, G. Chen, Z. Ren, Enhancement in thermoelectric figure-of-merit of an N-type half-Heusler compound by the nanocomposite approach, Adv. Energy Mater. 1 (2011) 643–647. doi:10.1002/aenm.201100126.

[6] X. Yan, W. Liu, S. Chen, H. Wang, Q. Zhang, G. Chen, Z. Ren, Thermoelectric property study of nanostructured p-type half-heuslers (Hf, Zr, Ti)CoSb0.8 Sn0.2, Adv. Energy Mater. 3 (2013) 1195–1200. doi:10.1002/aenm.201200973.

[7] T. Fu, X. Yue, H. Wu, C. Fu, T. Zhu, X. Liu, L. Hu, P. Ying, J. He, X. Zhao, Enhanced thermoelectric performance of PbTe bulk materials with figure of merit zT >2 by multi-functional alloying, J. Mater. 2 (2016) 141–149. doi:10.1016/j.jmat.2016.05.005.

[8] J.P. Heremans, V. Jovovic, E.S. Toberer, A. Saramat, K. Kurosaki, A. Charoenphakdee, S. Yamanaka, G.J. Snyder, Enhancement of Thermoelectric Efficiency in PbTe by Distortion of the Electronic Density of States, Science (80-.). 321 (2008) 1457–1461. doi:10.1126/science.1159725.

[9] L.D. Zhao, G. Tan, S. Hao, J. He, Y. Pei, H. Chi, H. Wang, S. Gong, H. Xu, V.P. Dravid, C. Uher, G.J. Snyder, C. Wolverton, M.G. Kanatzidis, Ultrahigh power factor and thermoelectric performance in hole-doped single-crystal SnSe, Science (80-.). 351 (2016) 141–144. doi:10.1126/science.aad3749.

[10] A.T. Duong, V.Q. Nguyen, G. Duvjir, V.T. Duong, S. Kwon, J.Y. Song, J.K. Lee, J.E. Lee, S. Park, T. Min, J. Lee, J. Kim, S. Cho, Achieving ZT=2.2 with Bi-doped n-type SnSe single crystals, Nat. Commun. 7 (2016) 1–6. doi:10.1038/ncomms13713.

[11] M. Benyahia, V. Ohorodniichuk, E. Leroy, A. Dauscher, B. Lenoir, E. Alleno, High thermoelectric figure of merit in mesostructured In0.25Co4Sb12 n-type skutterudite, J. Alloys Compd. 735 (2018) 1096–1104. doi:10.1016/j.jallcom.2017.11.195.

[12] H. Kim, S. Ballikaya, H. Chi, J.-P. Ahn, K. Ahn, C. Uher, M. Kaviany, Ultralow thermal conductivity of β-Cu2Se by atomic fluidity and structure distortion, Acta

Mater. 86 (2015) 247–253. doi:10.1016/J.ACTAMAT.2014.12.008.

[13] B. Yu, W. Liu, S. Chen, H.H. Wang, H.H. Wang, G. Chen, Z. Ren, Thermoelectric properties of copper selenide with ordered selenium layer and disordered copper layer, Nano Energy. 1 (2012) 472–478. doi:10.1016/J.NANOEN.2012.02.010.

[14] H. Liu, X. Shi, F. Xu, L. Zhang, W. Zhang, L. Chen, Q. Li, C. Uher, T. Day, G. Snyder Jeffrey, G.J. Snyder, Copper ion liquid-like thermoelectrics, Nat. Mater. 11 (2012) 422–425. doi:10.1038/nmat3273.

[15] P. Qiu, X. Shi, L. Chen, Cu-based thermoelectric materials, Energy Storage Mater. 3 (2016) 85–97. doi:10.1016/j.ensm.2016.01.009.

[16] T.R. Wei, C.F. Wu, F. Li, J.F. Li, Low-cost and environmentally benign selenides as promising thermoelectric materials, J. Mater. 4 (2018) 304–320. doi:10.1016/j.jmat.2018.07.001.

[17] L. Chen, J. Liu, C. Jiang, K. Zhao, H. Chen, X. Shi, L. Chen, C. Sun, S. Zhang, Y. Wang, Z. Zhang, Nanoscale Behavior and Manipulation of the Phase Transition in Single-Crystal Cu2Se, Adv. Mater. 31 (2019) 1–6. doi:10.1002/adma.201804919.

[18] S.D. Kang, J.-H. Pöhls, U. Aydemir, P. Qiu, C.C. Stoumpos, R. Hanus, M.A. White, X. Shi, L. Chen, M.G. Kanatzidis, G.J. Snyder, Enhanced stability and thermoelectric figure-of-merit in copper selenide by lithium doping, Mater. Today Phys. 1 (2017) 7–13. doi:10.1016/J.MTPHYS.2017.04.002.

[19] A. Bohra, R. Bhatt, S. Bhattacharya, R. Basu, S. Ahmad, A. Singh, D.K. Aswal, S.K. Gupta, Study of thermal stability of Cu2Se thermoelectric material, AIP Conf. Proc. 1731 (2016) 1–5. doi:10.1063/1.4948031.

[20] F.S. Liu, M.J. Huang, Z.N. Gong, W.Q. Ao, Y. Li, J.Q. Li, Enhancing the thermoelectric performance of β-Cu2Se by incorporating SnSe, J. Alloys Compd. 651 (2015) 648–654. doi:10.1016/j.jallcom.2015.08.154.

[21] R. Bhardwaj, A. Bhattacharya, K. Tyagi, B. Gahtori, N.S. Chauhan, A. Vishwakarma, K.K. Johari, S. Bathula, S. Auluck, A. Dhar, Enhancement in

thermoelectric performance of single step synthesized Mg doped Cu2Se: An experimental and theoretical study, Intermetallics. 112 (2019) 106541. doi:10.1016/j.intermet.2019.106541.

[22] A.A. Olvera, N.A. Moroz, P. Sahoo, P. Ren, T.P. Bailey, A.A. Page, C. Uher, P.F.P.P. Poudeu, Partial indium solubility induces chemical stability and colossal thermoelectric figure of merit in Cu2Se, Energy Environ. Sci. 10 (2017) 1668–1676. doi:10.1039/C7EE01193H.

[23] P. Peng, Z.N.N. Gong, F.S.S. Liu, M.J.J. Huang, W.Q.Q. Ao, Y. Li, J.Q.Q. Li, Structure and thermoelectric performance of β-Cu2Se doped with Fe, Ni, Mn, In, Zn or Sm, Intermetallics. 75 (2016) 72–78. doi:10.1016/J.INTERMET.2016.05.012.

[24] M. Li, S.M. Kazi Nazrul Islam, S. Dou, X. Wang, Significantly enhanced figure-of-merit in graphene nanoplate incorporated Cu2Se fabricated by spark plasma sintering, J. Alloys Compd. 769 (2018) 59–64. doi:10.1016/j.jallcom.2018.07.353.

[25] Z. Geng, D. Shi, L. Shi, Y. Li, G.J. Snyder, K. Lam, Conventional sintered Cu2-xSe thermoelectric material, J. Mater. (2019) 4–11. doi:10.1016/j.jmat.2019.06.005.

[26] L. Xue, Z. Zhang, W. Shen, H. Ma, Y. Zhang, C. Fang, X. Jia, Thermoelectric performance of Cu2Se bulk materials by high-temperature and high-pressure synthesis, J. Mater. 5 (2019) 103–110. doi:10.1016/j.jmat.2018.12.002.

[27] S. Butt, M.U. Farooq, W. Mahmood, S. Salam, M. Sultan, M.A. Basit, J. Ma, Y. Lin, C.W. Nan, One-step rapid synthesis of Cu2Se with enhanced thermoelectric properties, J. Alloys Compd. 786 (2019) 557–564. doi:10.1016/j.jallcom.2019.01.359.

[28] F.S. Liu, Z.N. Gong, M.J. Huang, W.Q. Ao, Y. Li, J.Q. Li, Enhanced thermoelectric properties of β-Cu2Se by incorporating CuGaSe2, J. Alloys Compd. 688 (2016) 521–526. https://www.sciencedirect.com/science/article/pii/S0925838816322538 (accessed September 4, 2019).

[29] M. Yao, W. Liu, X. Chen, Z. Ren, S. Wilson, Z. Ren, C. Opeil, Low temperature thermoelectric properties of p-type copper selenide with Ni, Te and Zn dopants, J. Alloys Compd. 699 (2017) 718–721. doi:10.1016/j.jallcom.2016.12.400.

[30] B.M. Bochentyn, J.L. Karczewski, T. Miruszewski, B. Kusz, Novel method for metal-oxide glass composite fabrication for use in thermoelectric devices, Mater. Res. Bull. 76 (2016) 195–204. doi:10.1016/j.materresbull.2015.12.018.

[31] B. Bochentyn, J. Karczewski, T. Miruszewski, B. Kusz, Structure and thermoelectric properties of Bi-Te alloys obtained by novel method of oxide substrates reduction, J. Alloys Compd. 646 (2015) 1124–1132. doi:10.1016/j.jallcom.2015.06.127.

[32] N. Gostkowska, T. Miruszewski, B. Trawiński, B. Bochentyn, B. Kusz, Structure and thermoelectric properties of Cs-Bi-Te alloys fabricated by different routes of reduction of oxide reagents, Solid State Sci. 73 (2017) 41–50. doi:10.1016/j.solidstatesciences.2017.07.016.

[33] B. Trawiński, B. Bochentyn, M. Łapiński, B. Kusz, A study of the kinetics of bismuth telluride synthesis by an oxide reduction method, Thermochim. Acta. 683 (2020) 178437. doi:10.1016/J.TCA.2019.178437.

[34] A. Le Bail, Whole powder pattern decomposition methods and applications: A retrospection, Powder Diffr. 20 (2005) 316–326. doi:10.1154/1.2135315.

[35] M. Singh, S. Bhan, Phase equilibria and crystal chemical relations in copper-nickel-selenium system, Prog. Cryst. Growth Charact. Mater. 20 (1990) 217–230. doi:10.1016/0960-8974(90)90002-A.

[36] E.J. Rees, C.D.A. Brady, G.T. Burstein, Solid-state synthesis of tungsten carbide from tungsten oxide and carbon, and its catalysis by nickel, Mater. Lett. 62 (2008) 1–3. doi:10.1016/j.matlet.2007.04.088.

[37] L. Yang, Z.-G. Chen, G. Han, M. Hong, Y. Zou, J. Zou, High-performance thermoelectric Cu2Se nanoplates through nanostructure engineering, Nano Energy. 16 (2015) 367–374. doi:10.1016/J.NANOEN.2015.07.012.

[38] J. Hu, X.A. Fan, C. Jiang, B. Feng, Q. Xiang, G. Li, Z. He, Y. Li, Introduction of

porous structure: A feasible and promising method for improving thermoelectric performance of Bi 2 Te 3 based bulks, J. Mater. Sci. Technol. (2018). doi:10.1016/j.jmst.2018.05.010.

FIGURE CAPTIONS

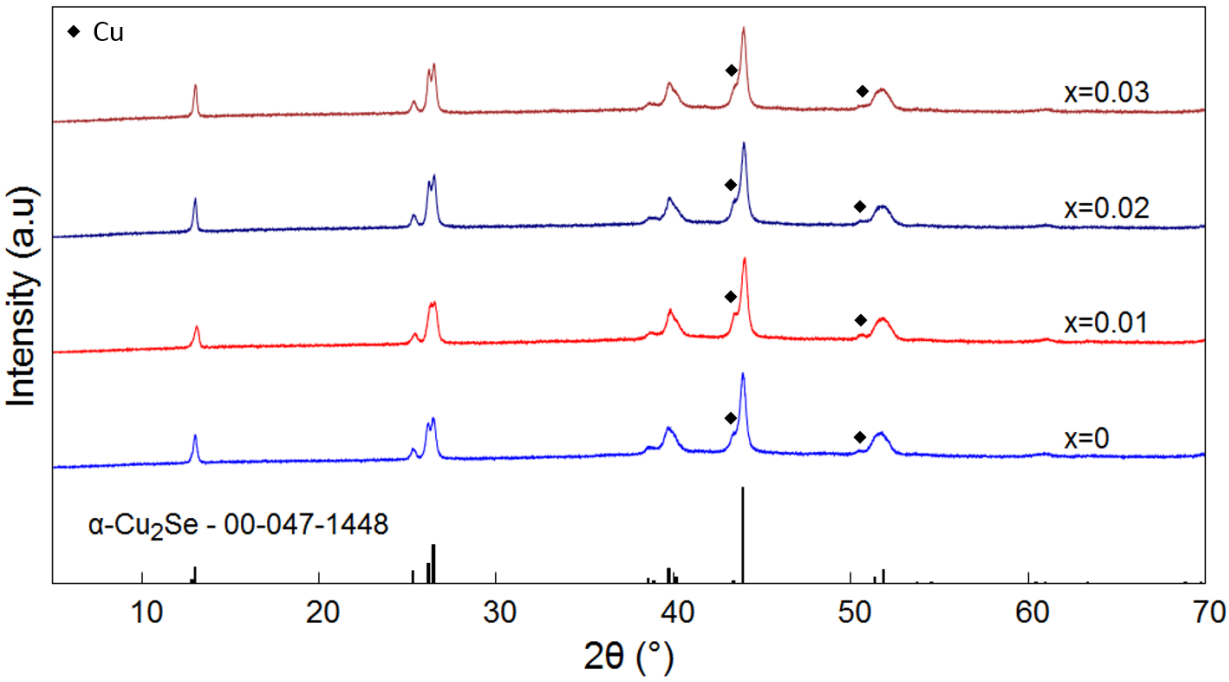

Fig. 1. XRD patterns of prepared $Cu_{2-x}Ni_xSe$ samples.

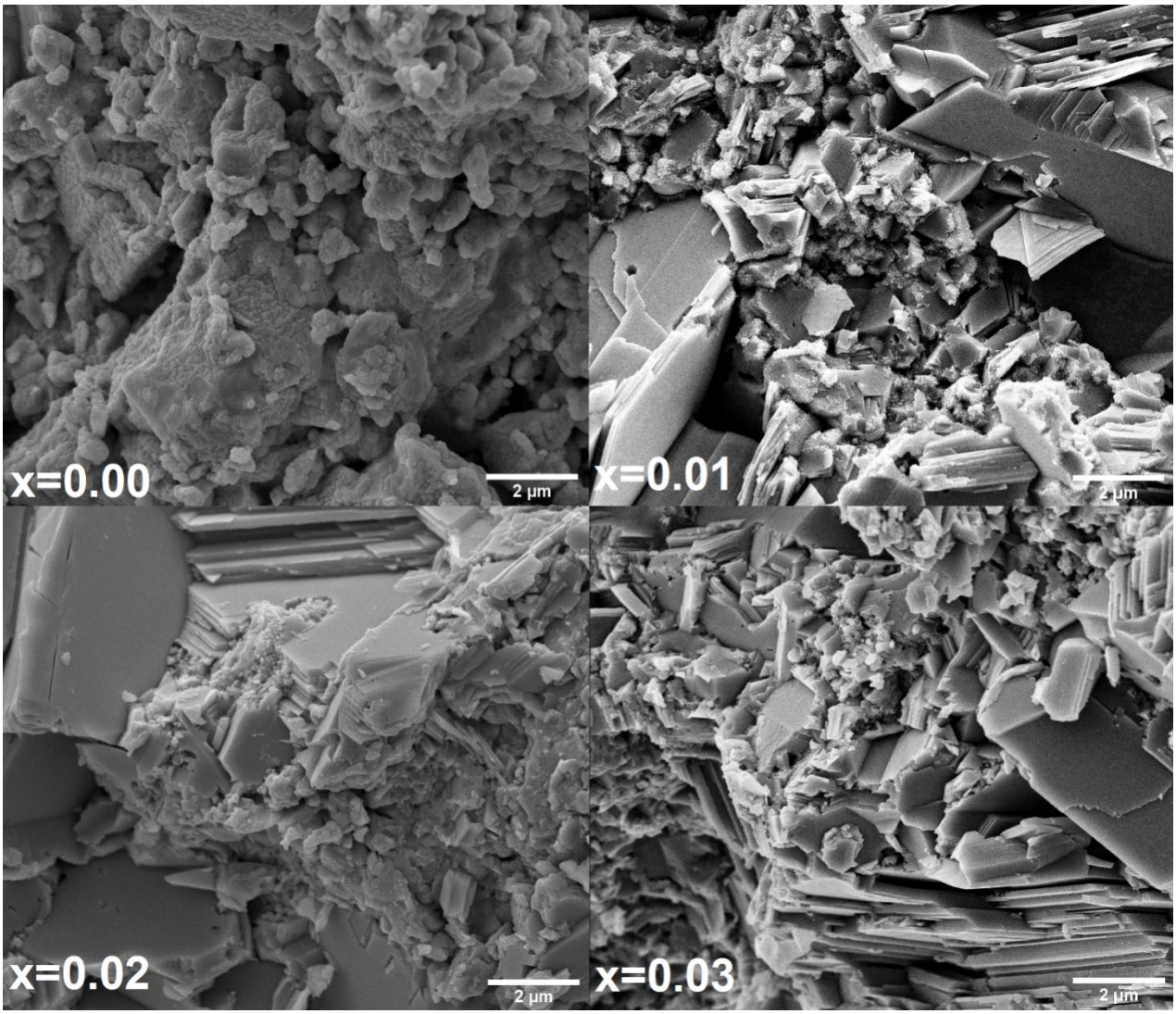

Fig. 2. SEM images of $Cu_{2-x}Ni_xSe$ samples.

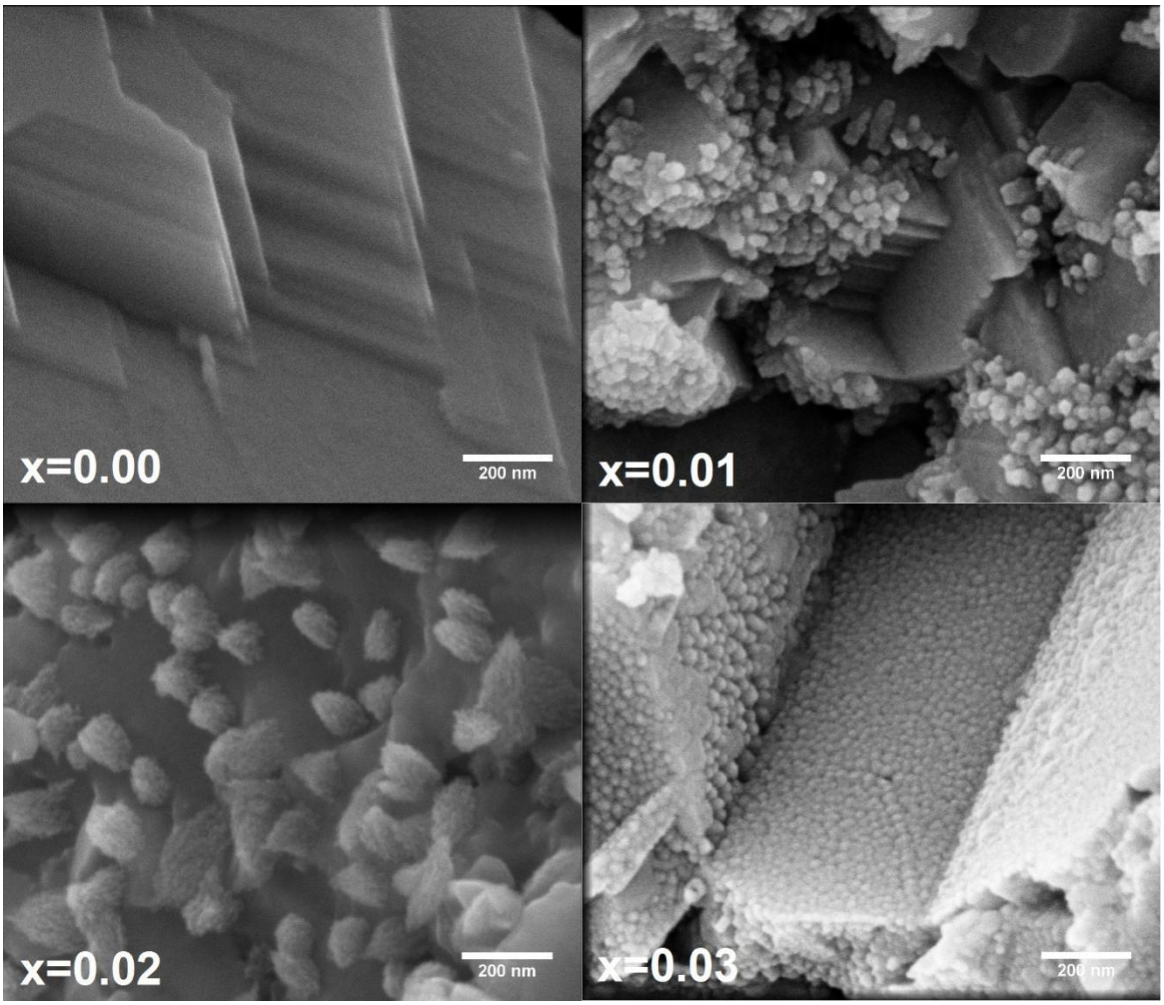

Fig. 3. SEM images of precipitations in samples with different Ni contents.

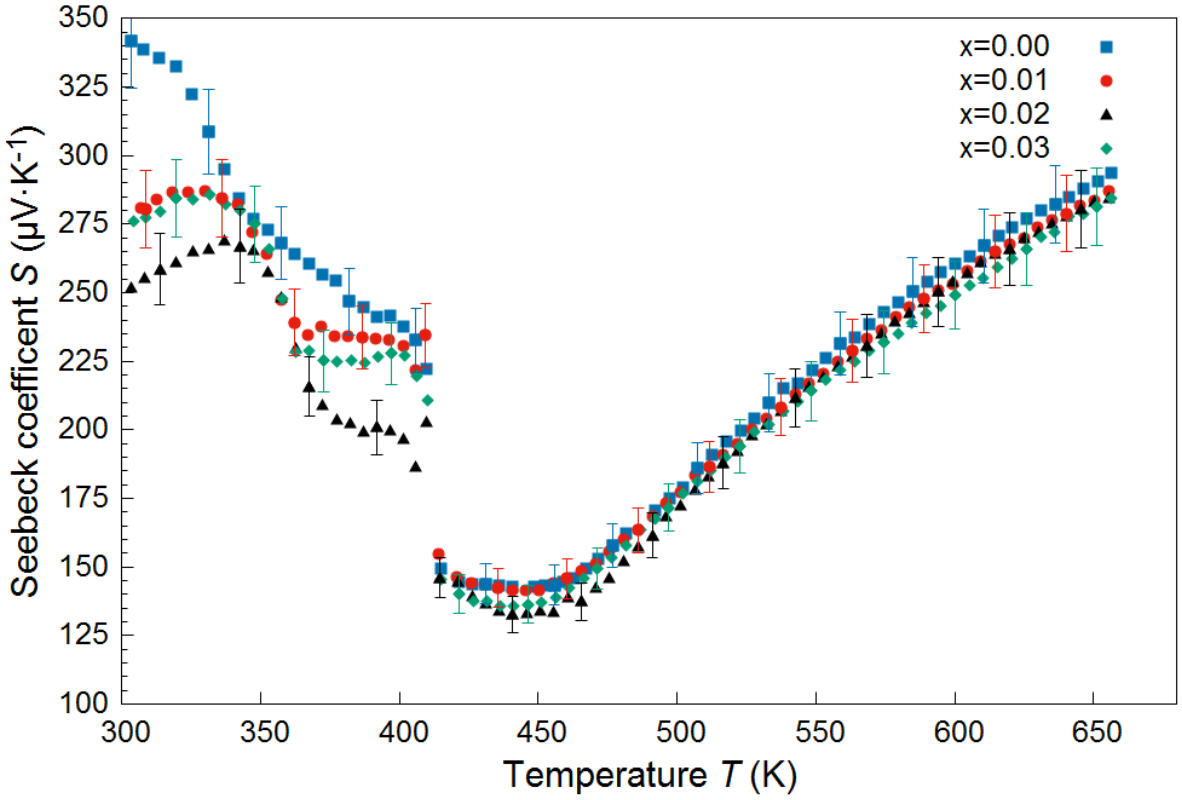

Fig. 4. Seebeck coefficient of $Cu_{2-x}Ni_xSe$ vs. temperature. For clarity, error bars are included for selected points only.

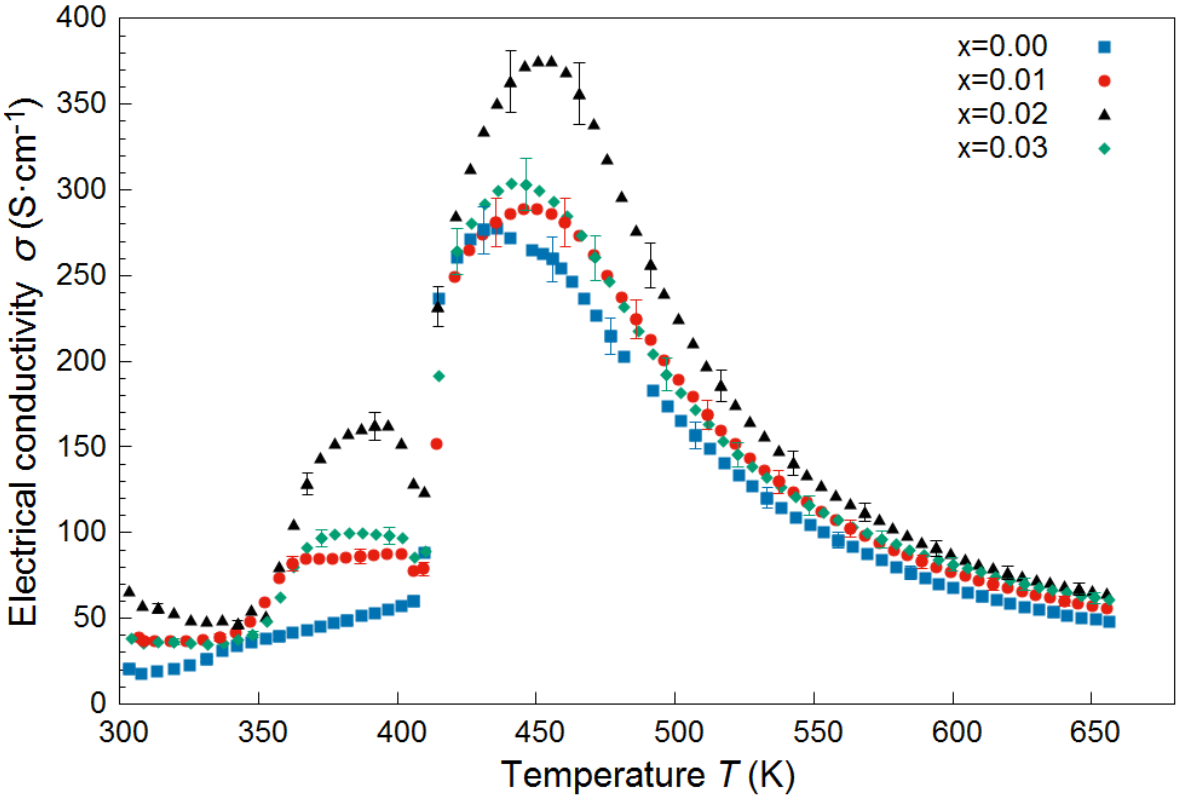

Fig. 5. Electrical conductivity of $Cu_{2-x}Ni_xSe$ vs. temperature. For clarity, error bars are included for selected points only.

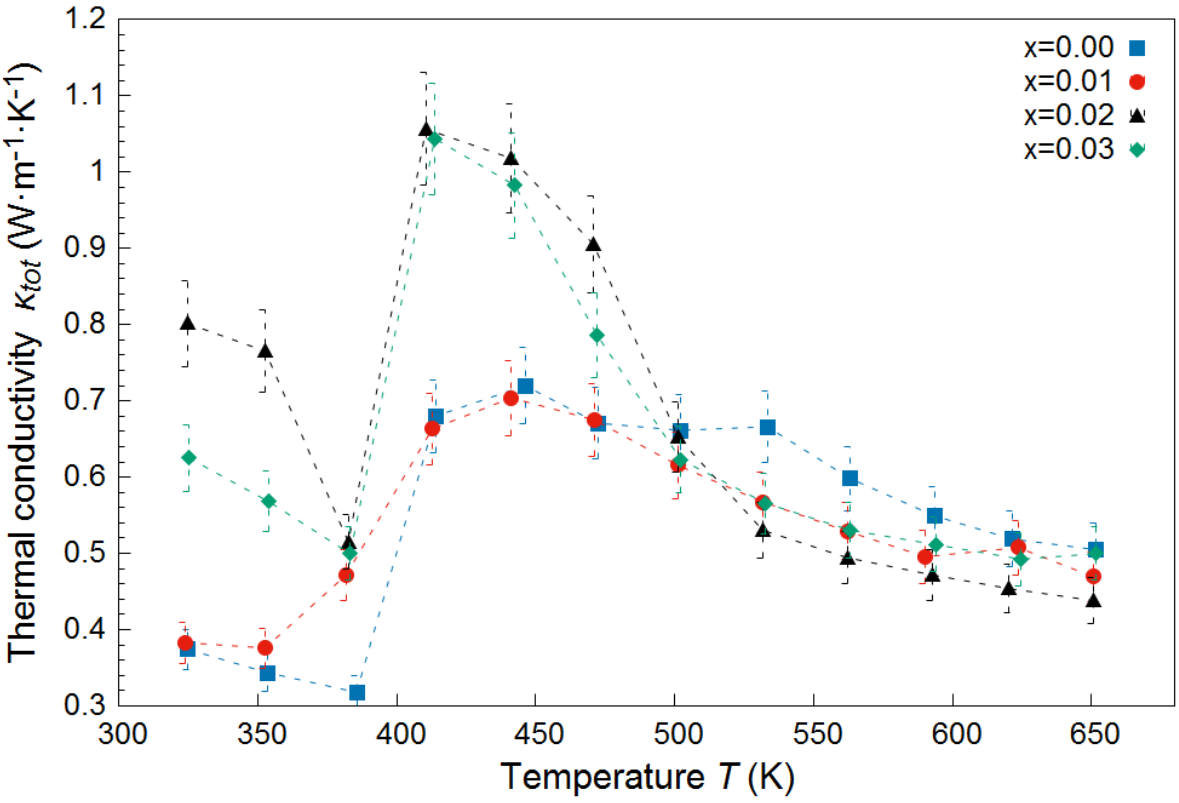

Fig. 6. Total thermal conductivity of $Cu_{2-x}Ni_xSe$. Dashed lines are visual guides only.

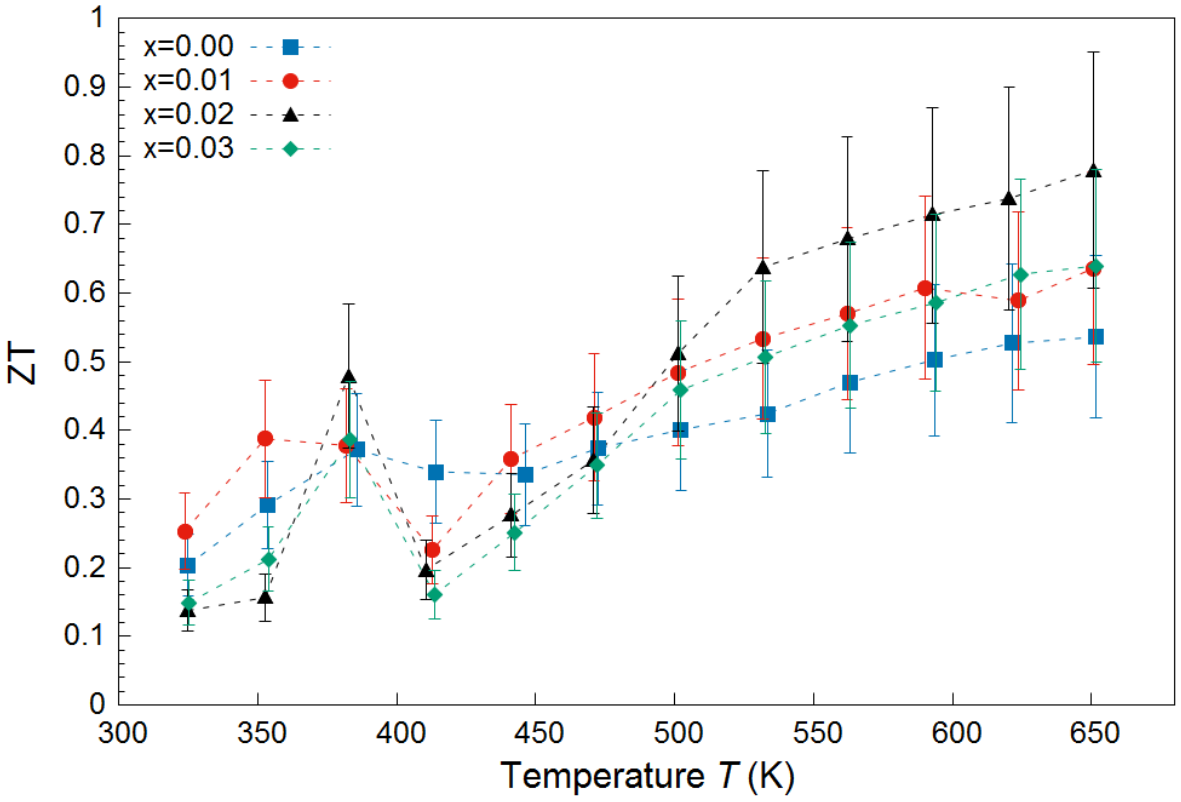

Fig. 7. Thermoelectric figure-of-merit of $Cu_{2-x}Ni_xSe$ vs. temperature. Dashed lines are visual guides only.

TABLES:

Tab. 1. Unit cell parameters of samples calculated from the Le Bail method.

Nominal sample composition	a (Å)	b (Å)	c (Å)	V (Å^3)
Cu_2Se	13.692(2)	20.468(4)	3.9271(8)	1100.594
$Cu_{1.99}Ni_{0.01}Se$	13.611(4)	20.391(5)	3.935(1)	1092.264
$Cu_{1.98}Ni_{0.02}Se$	13.589(3)	20.378(4)	3.8971(7)	1079.186
$Cu_{1.97}Ni_{0.03}Se$	13.643(3)	20.406(3)	3.9121(8)	1089.084

Tab. 2. Results of EDX area quantitative analysis

Nominal sample composition	EDX area composition	Porosity (%)
Cu_2Se	$Cu_{2.19}Se$	10
$Cu_{1.99}Ni_{0.01}Se$	$Cu_{2.13}Ni_{0.01}Se$	8
$Cu_{1.98}Ni_{0.02}Se$	$Cu_{2.19}Ni_{0.024}Se$	13
$Cu_{1.97}Ni_{0.03}Se$	$Cu_{2.14}Ni_{0.031}Se$	9